

Fluid velocity from transverse momentum spectra

Anthony Guillen¹ and Jean-Yves Ollitrault¹

¹*Institut de physique théorique, Université Paris Saclay, CNRS, CEA, F-91191 Gif-sur-Yvette, France*
(Dated: June 6, 2022)

We show that the momentum distributions calculated in ideal hydrodynamic simulations of nucleus-nucleus collisions are determined, to a good approximation, by the distribution of the transverse velocity of the fluid. We compute the fluid velocity distribution that gives the best fit to experimental data on Pb+Pb collisions at $\sqrt{s_{\text{NN}}} = 2.76$ TeV. We obtain reasonable fits up to $p_t \sim 6$ GeV, much beyond the range where hydrodynamics is usually applied. However, the fit is not perfect, even at low p_t . We actually argue that an ideal hydrodynamic calculation *cannot* fit simultaneously all identified particle spectra, irrespective of the specific implementation. In particular, data display a significant excess of pions at low p_t , whose physical interpretation is discussed. Data also show that the distribution of the fluid velocity becomes broader as the collision becomes less central. This broadening is explained by event-by-event hydrodynamic calculations, where it results from the centrality dependence of initial state fluctuations.

I. INTRODUCTION

The most fascinating aspect of ultrarelativistic nucleus-nucleus collisions is probably the formation of a tiny fluid droplet [1], whose temperature is the highest ever achieved in the laboratory [2], and which expands collectively before fragmenting into particles. It has long been known that this collective dynamics is imprinted into the momentum distributions of outgoing hadrons [3]. This is a less spectacular signature of collectivity than anisotropic flow [4–6], yet a direct and simple one.

We assess which information about the fluid can be obtained from measured transverse momentum (p_t) distributions, in a way that is robust with respect to details of hydrodynamic modeling. In Sec. II, we show that the momentum distribution from a full ideal hydrodynamic calculation is determined mostly by the distribution of the fluid velocity at freeze-out, and that the shape of the freeze-out hypersurface is relatively less important. This in turn means that if hydrodynamics is the correct description, then the distribution of the fluid velocity can be inferred from experimental results. In Sec. III, we evaluate this distribution using data from Pb+Pb collisions at $\sqrt{s_{\text{NN}}} = 2.76$ TeV collisions. We compare results obtained by fitting identified particle spectra, and unidentified, charged particle spectra. We point out generic discrepancies between ideal hydrodynamics and data, and discuss their possible interpretation, in particular in terms of dissipative corrections. In Sec. IV, we study the centrality dependence of p_t spectra. We extract the centrality dependence of the fluid velocity distribution from LHC data, and we compare with the centrality dependence calculated in event-by-event hydrodynamics.

II. IDEAL HYDRODYNAMICS AS A SUM OF BOOSTED THERMAL DISTRIBUTIONS

In a hydrodynamic simulation, one assumes that the system formed during the collision quickly equi-

brates [7]. The equations of relativistic hydrodynamics are used to model the subsequent expansion into the vacuum until the cohesion of the fluid is lost. The fluid then fragments into individual hadrons. We follow the usual simplified procedure where the transition from the fluid phase to free hadrons is an instantaneous freeze out [8–11], and rescatterings in the hadronic phase [12–15] are neglected. Hence, the output of the hydrodynamic calculation is a “freeze-out hypersurface” [16] from which particles are emitted. In this Section, we introduce an approximation to the usual freeze-out procedure which we dub “semi-Cooper–Frye” freeze out, and we test its validity using a realistic hydrodynamic calculation.

A. Why ideal hydrodynamics

Throughout this paper, we use ideal hydrodynamics, not viscous hydrodynamics. This means in practice that particles are emitted according to a thermal distribution in the rest frame of the fluid [17]. There are two reasons for this choice.

The first reason is that the validity of hydrodynamics implies that the departure from thermal equilibrium is small: Hydrodynamics is a gradient expansion [18, 19], where ideal hydrodynamics is the leading term, and Navier–Stokes viscous hydrodynamics represents the first-order correction. While the first-order correction is significant for anisotropic flow [20], it is known to be modest for the transverse momentum distributions, averaged over azimuthal angle [21], which we study here.

The second reason is that the deviations from the thermal distribution are not solely determined by the viscosity (shear and bulk). They depend on the underlying microscopic transport processes [22], such as hadronic interactions at freeze out [9, 23], which are not constrained. One of our goals is to obtain direct information on these deviations from experimental data, by studying how data deviate from the ideal-fluid picture. We come back to this in Sec. III B.

B. Cooper–Frye freeze out

The distribution of hadrons at freeze out is given by the Cooper–Frye formula [8]:

$$\frac{dN}{d^3p} = \frac{2S+1}{(2\pi)^3} \int_{\sigma} \frac{1}{e^{E^*/T_f} \pm 1} \frac{p^\mu}{p^0} d\sigma_\mu, \quad (1)$$

where p^μ is the four-momentum ($p^0 = \sqrt{\vec{p}^2 + m^2}$), u^μ is the fluid four-velocity [17], $E^* \equiv p^\mu u_\mu$ denotes the energy of the hadron in the rest frame of the fluid, T_f is the freeze-out temperature, and the integral runs over the freeze-out hypersurface σ , whose infinitesimal area vector is $d\sigma_\mu$. $2S+1$ denotes the number of independent spin states, and the $+$ and $-$ signs apply to baryons (half-integer S) and mesons (integer S), respectively. We only discuss ultrarelativistic energies, where the baryon chemical potential μ_B is negligible.

If freeze out occurs at a constant time, only $d\sigma_0$ is non-vanishing, and the factor p^μ/p^0 is unity. Then, the momentum distribution is simply a sum of thermal distributions, boosted by the fluid velocity. By contrast, for a fluid flowing through a fixed surface, corresponding to the spatial components $d\vec{\sigma}$, the thermal distribution is multiplied by the velocity of the particle \vec{p}/p^0 . Hence, the particle distribution in ideal hydrodynamics is not solely determined by the temperature and the fluid velocity. It also involves the orientation of the freeze-out hypersurface in space-time.

C. Semi-Cooper–Frye freeze out

We introduce a simplified version of the Cooper–Frye formula (1), where we evaluate the flux by approximating the particle velocity \mathbf{p}/p^0 with the fluid velocity \mathbf{u}/u^0 :

$$\frac{dN}{d^3p} = \frac{2S+1}{(2\pi)^3} \int_{\sigma} \frac{1}{e^{E^*/T_f} \pm 1} \frac{u^\mu}{u^0} d\sigma_\mu. \quad (2)$$

This expression coincides with (1) for massive particles in the low-temperature limit, where the thermal velocity is negligible compared to the fluid velocity [24]. Note that unlike Eq. (1), Eq. (2) is not invariant under Lorentz transformations.¹ Lorentz invariance is however irrelevant here because Eq. (2) is merely an approximation which we use only in a specific reference frame, which will be defined below. We dub the approximation (2) ‘‘semi-Cooper–Frye’’ freeze out because it coincides with the

¹ Lorentz invariance can be preserved by replacing p^μ/p^0 with E^*u^μ/p^0 in Eq. (1). We have checked numerically that this Lorentz-invariant approximation is worse than our semi-Cooper–Frye approximation. The reason is that it is also wrong for the space-like portion of the freeze-out hypersurface, where semi-Cooper–Frye is exact. Note that the Cooper–Frye formula [8] was precisely introduced as a replacement to this Lorentz-invariant approximation [25].

Cooper–Frye formula only for the space-like part of the hypersurface.² Its validity will be tested in Sec. II F.

The distribution (2) can be rewritten as an integral over the fluid velocity $\mathbf{u} = (u_x, u_y, u_z)$:

$$\frac{dN}{d^3p} = \frac{2S+1}{(2\pi)^3} \int \frac{1}{e^{E^*/T_f} \pm 1} \Omega(\mathbf{u}) d\mathbf{u}, \quad (3)$$

where $\Omega(\mathbf{u})d\mathbf{u}$ is defined as:

$$\Omega(\mathbf{u})d\mathbf{u} = \int_{\sigma, \mathbf{u} \text{ in } d\mathbf{u}} \frac{u^\mu}{u^0} d\sigma_\mu. \quad (4)$$

In Eq. (4), the integral runs only on the part of the freeze-out hypersurface σ where the fluid velocity is \mathbf{u} up to $d\mathbf{u}$. If freeze-out occurs at a constant time, only the $\mu = 0$ component contributes, and $\Omega(\mathbf{u})d\mathbf{u}$ is simply the volume of the fluid with velocity \mathbf{u} up to $d\mathbf{u}$. The more general expression (4) can be thought of as an effective volume. Equation (3) expresses the momentum distribution as a weighted sum of boosted thermal distributions, and the information about the freeze-out hypersurface is encoded in the weight $\Omega(\mathbf{u})$.

D. Adding decays

Unstable hadrons decay before reaching the detectors, and the measured momentum distributions are those of the decay products at the end of the decay chain. We evaluate the momentum distribution of these decay products using the method recently introduced by Mazeliauskas *et al.* [28]. It amounts to carrying out the following replacement in the Cooper–Frye formula (1):

$$\frac{1}{e^{E^*/T_f} \pm 1} \frac{p^\mu}{p^0} \rightarrow f_1(E^*) \frac{p^\mu}{p^0} + (f_2(E^*) - f_1(E^*)) \frac{E^* u^\mu}{p^0}, \quad (5)$$

where $f_1(E^*)$ and $f_2(E^*)$ are two Lorentz scalar functions which are computed for each stable hadron, and depend on the freeze-out temperature T_f . They take into account the whole decay chain. If there are no decays, then $f_2(E^*) = f_1(E^*) = (e^{E^*/T_f} \pm 1)^{-1}$, and the left-hand side and right-hand side of (5) coincide.

Semi-Cooper–Frye freeze out can be readily generalized to include these decays. We again approximate the particle velocity p^μ/p^0 with the fluid velocity u^μ/u^0 in the first term of the right-hand side of (5). This amounts to replacing

$$\frac{1}{e^{E^*/T_f} \pm 1} \rightarrow f_1(E^*) + (f_2(E^*) - f_1(E^*)) \frac{E^* u^0}{p^0} \quad (6)$$

in Eqs. (2) and (3). The expression of the effective volume (4) is unchanged.

² Note that the semi-Cooper–Frye ansatz automatically solves the problem of negative contributions in Eq. (1) [26, 27], because the fluid typically flows outwards. The price to pay is a slight violation of energy and momentum conservation.

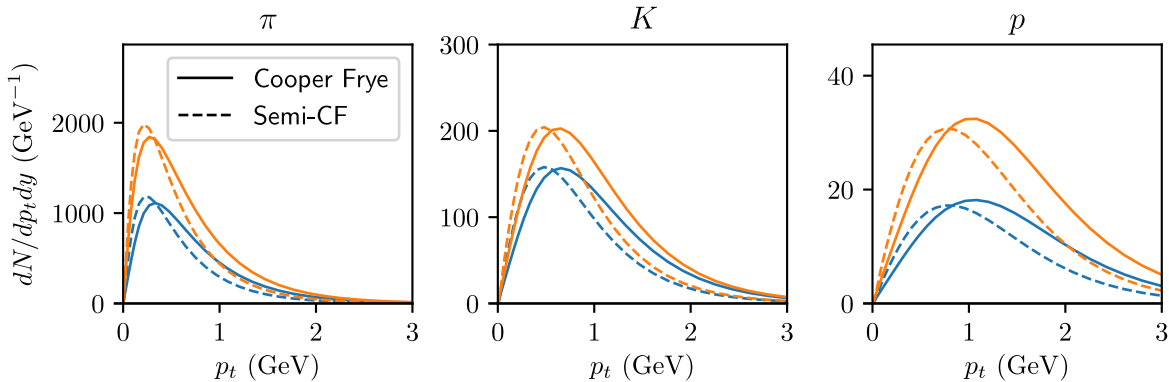


FIG. 1. (Color online) Comparison between p_t spectra calculated using the usual Cooper–Frye formula (1) (full lines), and the semi-Cooper–Frye approximation (2) (dashed lines), before (blue lines) and after decays (orange lines). From left to right: Charged pions, charged kaons, protons plus antiprotons. These results are obtained for a simulation of a central Pb+Pb collision at $\sqrt{s_{NN}} = 2.76$ TeV with the initial condition model TRENTo [29]. Initial-state fluctuations are simulated, but we only pick one random collision event. After a thermalization time $\tau_0 = 0.4$ fm/c [30], we evolve this initial condition through 2+1 dimensional boost-invariant ideal hydrodynamics using the MUSIC code [31–33] with a realistic equation of state inspired by lattice QCD [34]. The freeze-out temperature is $T_f = 135$ MeV (see Sec. III A).

E. Transverse momentum distribution

From now on, our study is restricted to the transverse momentum distribution, dN/dp_t , which is obtained by integrating over the longitudinal momentum and the azimuthal angle:

$$\frac{dN}{dp_t} = p_t \int_{-\infty}^{+\infty} dp_z \int_{-\pi}^{\pi} d\phi \frac{dN}{d^3p}. \quad (7)$$

We now evaluate dN/dp_t using the semi-Cooper–Frye approximation. p_t is invariant under longitudinal Lorentz boosts, but the semi-Cooper–Frye approximation is not. Therefore, we need to specify the frame where it is applied. We choose the reference frame where $u_z = 0$, i.e., the fluid is at midrapidity.³ Then, the momentum distribution is given by Eq. (3), where

$$E^* \equiv \sqrt{(1+u^2)(m^2 + p_z^2 + p_t^2)} - up_t \cos(\phi - \phi_u). \quad (8)$$

In this equation, ϕ_u denotes the azimuthal angle of the fluid velocity, and u the transverse fluid velocity:

$$u \equiv \sqrt{u_x^2 + u_y^2}. \quad (9)$$

Since the p_t distribution (7) is integrated over ϕ , one can set $\phi_u = 0$ in Eq. (8) without any loss of generality.

Therefore, the p_t distribution only involves the distribution of the transverse velocity u .

Inserting Eqs. (3) and (8) into Eq.(7), we thus rewrite the p_t distribution as integral over u :

$$\frac{dN}{dp_t} = \int_0^\infty f(p_t, u) \Omega(u) du, \quad (10)$$

where $\Omega(u)du$ represents the effective freeze-out volume whose transverse velocity lies between u and $u + du$, obtained by integrating Eq. (4) on u_z and ϕ_u :

$$\Omega(u)du = \int_{\sigma, u \text{ in } du} \frac{u^\mu}{\sqrt{1+u^2}} d\sigma_\mu \quad (11)$$

(note that the $\mu = z$ component is zero by choice of the reference frame), and $f(p_t, u)$ is a boosted thermal distribution:

$$f(p_t, u) \equiv \frac{2S+1}{(2\pi)^3} p_t \int_{-\infty}^{+\infty} dp_z \int_{-\pi}^{\pi} d\phi \frac{1}{e^{E^*/T_f} \pm 1}. \quad (12)$$

Resonance decays are taken into account through the substitution (6).

Equation (10) expresses the p_t distribution as a sum of boosted thermal distributions. Hence, the semi-Cooper–Frye approximation can be seen as a generalization of the blast-wave parametrization [35–37], which is commonly used to fit p_t spectra [38, 39]. Blast-wave calculations are less general in the sense that they typically assume a specific functional form for the distribution $\Omega(u)$ of the fluid velocity u at freeze-out.⁴

³ Since the fluid typically extends over a range of rapidities, this implies in practice that we slice the fluid according to rapidity, and evaluate dN/dp_t separately in each slice.

⁴ Note that blast-wave calculations can be improved to take into account the shape of the freeze-out hypersurface [40].

F. Testing the semi-Cooper–Frye approximation

We test the validity of the semi-Cooper–Frye approximation by comparing with the results of the standard Cooper–Frye procedure for an ideal hydrodynamic simulation of a central Pb+Pb collision at $\sqrt{s_{\text{NN}}} = 2.76$ TeV. Our simulation assumes longitudinal boost invariance [41]. Hence, the hypersurface element $d\sigma_\mu$ must be understood as “per unit rapidity”, and so is the resulting momentum distribution. Therefore, dN/dp_t in (10) actually stands for $dN/dydp_t$, where y is the rapidity. Resonance decays are implemented using the FastReso code [28]. The semi-Cooper–Frye approximation is implemented by first evaluating the distribution of the transverse fluid velocity at freeze-out using Eq. (11), and then computing the spectra using Eq. (10).

The comparison with the usual Cooper–Frye result is displayed in Fig. 1. One sees that the semi-Cooper–Frye approximation overestimates the particle yield at low p_t and underestimates it at high p_t , compared to the full Cooper–Frye treatment. This can be readily understood by comparing the corresponding equations: Eq. (2) overestimates or underestimates the particle yield, relative to Eq. (1), depending on whether the fluid velocity \vec{u}/u^0 is larger or smaller than the particle velocity \vec{p}/p^0 .

It is interesting to note that the difference between the dashed lines and the full lines in Fig. 1 represents the difference between a blast-wave parametrization and a full hydrodynamic calculation, since the semi-Cooper–Frye approximation can be seen as a generalization of the blast-wave approach. Hence, a blast-wave calculation typically overestimates the particle yield at low p_t and underestimates it at high p_t . One may think that the error is not negligible. However, one should keep in mind that spectra are usually shown on a logarithmic scale. As we shall see, the discrepancies between hydrodynamics and experimental data are typically larger than the error introduced by the semi-Cooper–Frye approximation. Hence, we deem semi-Cooper–Frye freeze-out a decent approximation for our purpose.

III. DISTRIBUTION OF FLUID VELOCITY FROM LHC DATA

We now explain how the distribution of the transverse fluid velocity at freeze-out, $\Omega(u)$, can be extracted from experimental data. As in the vast majority of hydrodynamical simulations [9–11, 14, 15], we assume that freeze-out occurs at a fixed temperature T_f . The value of T_f relevant to our calculation is determined in Sec. III A. Then, within the semi-Cooper–Frye approximation, $\Omega(u)$ can be obtained by fitting the transverse momentum distribution dN/dp_t using Eq. (10). We first carry out a combined fit of data on pion, kaon, proton spectra in Sec. III B. In Sec. III C, we compare the value of $\Omega(u)$ from data with that obtained in state-of-the-art calculations. Fits to unidentified hadron spectra are discussed

in Sec. III D.

A. Freeze-out temperature

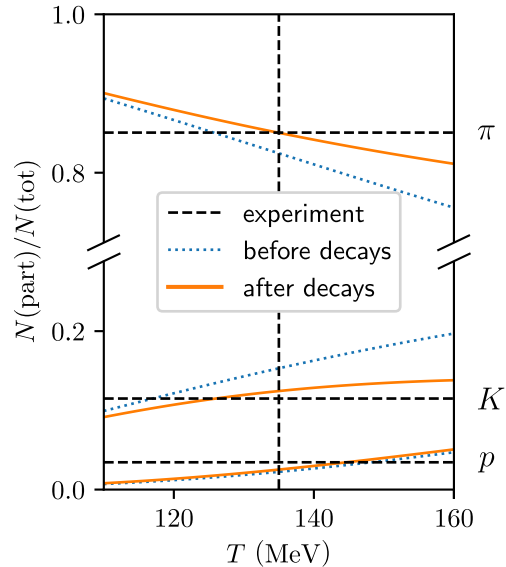


FIG. 2. (Color online) Relative abundances of charged pions, kaons, and protons, before (dotted lines) and after (full line) resonance decays [28] for a fluid at rest, as a function of its temperature T_f . These relative abundances add up to unity by construction. The horizontal dashed lines correspond to the experimental values, obtained by integrating the spectra in 0-5% central Pb+Pb collisions at $\sqrt{s_{\text{NN}}} = 2.76$ TeV [42]. The range of the integration over p_t in our calculation is the same as in experiment. The vertical line corresponds to the value $T_f = 135$ MeV which we choose throughout this article.

We consider for simplicity a single freeze-out model [9, 43] where chemical and kinetic freeze-out occur simultaneously at temperature T_f . In other terms, we do not implement partial chemical equilibration [10, 44, 45]. Equation (10) then defines not only the probability distribution of p_t for a given hadron, but also its normalization. Since we are going to fit the spectra of pions, kaons and protons [39, 42], we must choose a value of T_f which fits their relative abundances, obtained by integrating the spectra. Figure 2 displays the relative abundances of these particles as a function of T_f for a fluid at rest. The choice $T_f = 135$ MeV gives reasonable agreement with experiment, once the feeddown from resonance decays is taken into account. We choose this value throughout this article.⁵ Devetak *et al.* [46] obtain a similar value

⁵ Note that the relative abundances are strictly independent of

(137 MeV) through a global fit to pion, kaon, proton spectra.⁶

Note that our value of T_f is significantly smaller than the usual value $T_c = 156$ MeV of the chemical freeze-out temperature [49], obtained by fitting the relative abundances of *all* hadrons. This higher temperature is mostly dictated by relative abundances of strange baryons [50]. But we do not study strange baryons here, and they represent a small fraction of the particle yield anyway (see Sec. III D for the case of Σ baryons).

Note also that our approach differs from usual blast-wave fits, where the freeze-out temperature is fitted independently for each hadron species [38, 39]. Our goal is to mimic a hydrodynamic calculation, where the freeze-out temperature is common to all hadrons, and determines both the spectra and the relative yields.

B. Fits to identified particle spectra

We carry out a combined fit of pion, kaon and proton spectra measured in Pb+Pb collisions at $\sqrt{s_{\text{NN}}} = 2.76$ TeV [42] up to $p_t = 7$ GeV/c using Eq. (10). The validity of the fitting algorithm has first been tested using artificially-generated data, as explained in Appendix A. We use same fitting function $\Omega(u)$ for all particle species. It defines their p_t distribution, including the normalization. The procedure is repeated in every centrality window. Fig. 3 displays the measured spectra together with the fits. Data are above the model at high p_t , as expected for thermal models. Note, however, that the deviations become large only for $p_t > 6$ GeV. This is much higher than the typical p_t range used in hydrodynamic calculations [46, 51–53] or blast-wave fits [37, 54], which typically does not extend beyond $p_t \sim 2 - 3$ GeV. It is interesting to note that our simple generalization of the blast-wave approach allows us to greatly improve agreement with data all the way to 6 GeV. The reason will be discussed in Sec. III C.

Deviations between the fit and data also appear at lower transverse momentum. Data show an excess of pions for $p_t < 1$ GeV/c, followed by a depletion up to $p_t \sim 3$ GeV, and an excess of protons for $p_t > 1$ GeV/c. Similar deviations appear in other blast-wave fits [37, 54].

We now discuss whether the discrepancy between data and ideal hydrodynamics can be attributed to the approximate treatment of freeze out introduced in Sec. II C. Fig. 1 shows that semi-Cooper–Frye freeze out overestimates the hadron yield at low p_t and underestimates it

at high p_t , compared to a full hydrodynamic calculation. Therefore, if data show an excess at low p_t compared to the result of semi-Cooper–Frye, as seen for pions in Fig. 3, the excess is likely to be even worse when comparing to a full hydrodynamic calculation. On the other hand, one may hope that the high- p_t proton excess will be fixed by the full Cooper–Frye calculation. These expectations are confirmed by the recent study of Devetak *et al.* [46], which is a full hydrodynamic calculation, also including viscosity. The proton excess above 1.5 GeV/c is no longer apparent, and the most notable deviation between data and hydrodynamics is the excess of pions for $p_t < 0.5$ GeV/c, which is present for all centralities, and already well known [52, 55].

Our study shows that the pion excess at low p_t relative to ideal hydrodynamics is a general result, which cannot be fixed by tuning the parameters of the hydrodynamic calculation. This excess is still present even though we took into account the feeddown from resonance decays, whose contribution is essential at low p_t . The natural expectation would be that the excess is explained by the leading correction to ideal hydrodynamics, namely, viscous hydrodynamics. As recalled in Sec. II A, the viscous correction to the thermal distribution is not universal. It depends on momentum through details of hadron cross sections. Essentially *all* viscous hydrodynamic calculations [46, 51–53] assume for simplicity that the momentum dependence is quadratic [56], which in turn implies that the departure from thermal equilibrium is larger at high p_t . This quadratic ansatz makes hydrodynamic calculations of anisotropic flow look better at high p_t [21], but lacks a microscopic justification [22, 23].

Our comparison to data suggests instead that the departure from thermal equilibrium is larger for low momentum pions. This actually makes sense from a theoretical point of view. It has long been known that low-momentum pions are Goldstone bosons [57, 58] which interact little. It has been recently argued that they could be treated as superfluid degrees of freedom [59].

C. Distribution of fluid velocity

We now discuss the results for the fitting function $\Omega(u)$, whose value is returned by the fits to identified particle spectra. In order to limit the number of fit parameters, we have assumed that u takes discrete values spaced with a step $\Delta u = 0.4$. The corresponding $\Omega(u)$ is a sum of Dirac peaks centered at the corresponding values of u , which we represent in Fig. 4 as a step function with the same area. The values of $\Omega(u)$ given by the fits of Fig. 3 are represented in Fig. 4. As explained in Sec. II E, $\Omega(u)$ represents the distribution of the transverse 4-velocity u . One sees that the most probable values of u are around unity, corresponding to a fluid moving at 70% of the velocity of light. The integral $V_{\text{eff}} \equiv \int \Omega(u) du$ is the effective volume at freeze out. It represents the volume of a hadron gas at $T_f = 135$ MeV such that the multiplicity is

the fluid velocity if integrated over all p_t . In Fig. 2, however, we implement the same p_t cuts as in experiment. Therefore, the relative abundances are no longer strictly independent of the fluid velocity, but we neglect this dependence.

⁶ Note that relative yields are somewhat modified if one takes into account finite resonance widths [47] and pion-nucleon interactions [48], which are both neglected here.

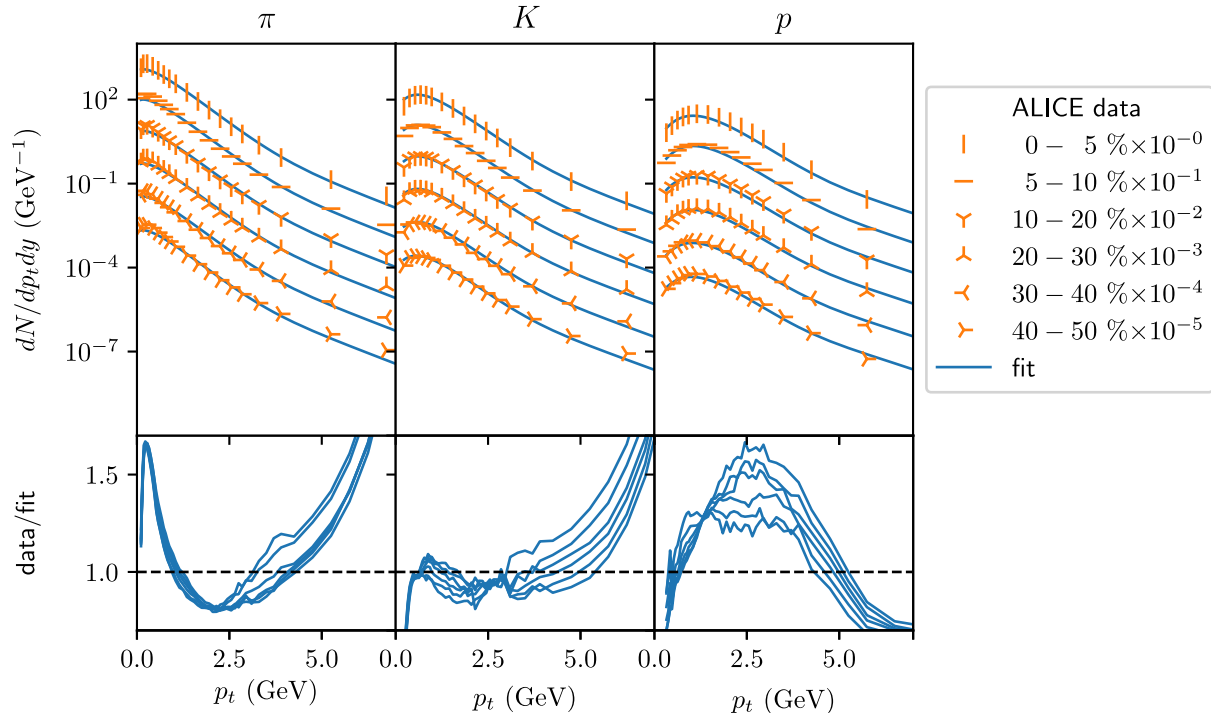


FIG. 3. (Color online) Symbols: p_t distributions of charged pions, charged kaons and protons measured by ALICE [42] in Pb+Pb collisions at $\sqrt{s_{\text{NN}}} = 2.76$ TeV, in several centrality windows. Lines: Fits using Eq. (10). For each centrality, the function $\Omega(u)$ is fitted so as to achieve the best simultaneous fit of pion, kaon, proton spectra in the range $0 < p_t < 7$ GeV/c. The bottom panels display the ratio data/fit.

the same as in data. Therefore, its centrality dependence follows that of the charged multiplicity [60].

Note also that $\Omega(u)$ has a non-zero value in the highest velocity bin $2.6 < u < 3$, corresponding to collective velocities in the range 93–95% of the velocity of light. $\Omega(u)$ in this bin is very small, yet the corresponding contribution becomes dominant at high p_t . This is the “trick” that enables the fitting algorithm to fit data all the way up to $p_t \sim 6$ GeV. Usual blast-wave fits use a smooth $\Omega(u)$, whose support (the range in u where $\Omega(u) > 0$) is much smaller, and fail typically beyond 2 GeV.

For the sake of comparison with the result of our fit, we now evaluate $\Omega(u)$ in a state-of-the-art ideal hydrodynamic simulation of Pb+Pb collisions at $\sqrt{s_{\text{NN}}} = 2.76$ TeV, which we now describe. We use boost-invariant [41] initial conditions, with a starting time $\tau_0 = 0.4$ fm/c. The transverse velocity at τ_0 is set to zero, that is, initial flow [61, 62] is neglected. In order to model event-to-event fluctuations, we model the entropy density at τ_0 using the TRENTo Monte Carlo generator [29] with the $p = 0$ prescription (corresponding to an entropy density proportional to $\sqrt{T_A T_B}$, where T_A and T_B are the thickness functions of incoming nuclei [63]), which has been employed successfully in phenomenological applications [64]. The entropy density profile is normalized so

that the multiplicity per unit rapidity in central collisions matches the value extracted from experimental data [65]. We then evolve this initial condition using the MUSIC hydrodynamic code [31–33] with a realistic equation of state inspired by lattice QCD [34]. Freeze out is done at $T_f = 135$ MeV as discussed in Sec. III A. We do not implement Cooper–Frye freeze out. Instead, we directly obtain $\Omega(u)$ from Eq. (11), where the integration runs over the freeze-out hypersurface.

The maximum of $\Omega(u)$ is at $u \simeq 1$ in the hydrodynamic calculation, as in the value extracted from data. The effective volume $\int \Omega(u) du$ is also comparable, which is a consequence of the fact that the hydrodynamic model predicts the correct multiplicity. The most striking difference with the value extracted from experimental data is that data prefer a narrower distribution.

It is instructive to understand qualitatively how the distribution of the fluid velocity, $\Omega(u)$, relates to the p_t spectra. The transverse momentum of a particle emitted at a given point of the freeze-out hypersurface results from the superposition of the collective motion and the random thermal motion [17], $p_t = mu + p_{\text{th}}$, where p_{th} is the thermal momentum. The higher the mass, the smaller the thermal component relative to the collective one. Therefore, one expects the distribution of u to ap-

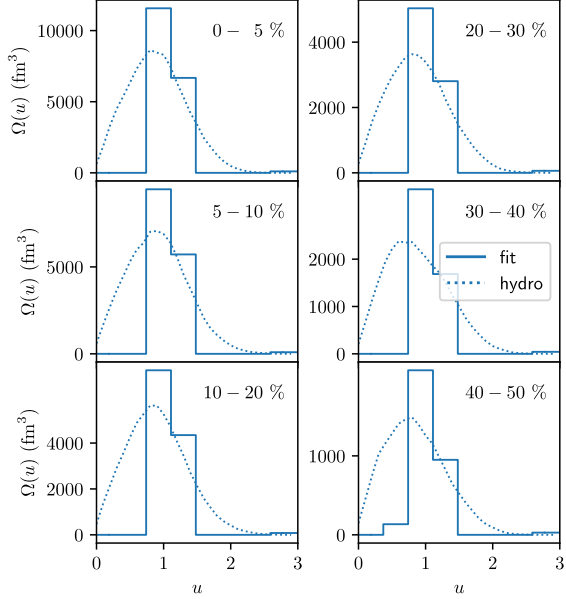


FIG. 4. (Color online) Full lines: Values of $\Omega(u)$ given by the fits of Fig. 3. We have assumed that u takes discrete values with a step $\Delta u = 0.4$. The integral $V_{\text{eff}} \equiv \int_{u=0}^{\infty} \Omega(u) du$ is an effective volume per unit rapidity at freeze-out, hence the unit fm^3 on the vertical axis. Dotted curves: $\Omega(u)$ in an event-by-event ideal hydrodynamic calculation with T_{RE}NTO initial conditions (see text).

proach the distribution of p_t/m for massive particles [24]. Fig. 5 presents the normalized probability distribution of p_t/m for pions, kaons, protons, deuterons, together with the discrete distribution of the fluid velocity extracted from a combined fit to these spectra, and with the continuous distribution of the fluid velocity from our hydrodynamic calculation. Note that deuterons were not included in Figs. 3 and 4, because we wanted to make use of the finer centrality binning which is available for the three lighter species. Deuterons are useful here, because their velocity distribution comes closer to that of the fluid velocity u , due to their much higher mass. The coarse binning in the fluid velocity u used for the fits partially hides this correspondence, but it is clearly seen when comparing the deuteron spectrum with the smooth distribution of u from the hydrodynamic calculation.

D. Unidentified spectra and the low- p_t pion excess

We now investigate whether the distribution of the fluid velocity can be extracted from unidentified charged particle spectra, which are easier to measure, and for which a broader range of data is available [67, 69]. We first carry out a preliminary check on ALICE data. We check if the charged particle spectrum [67] matches with

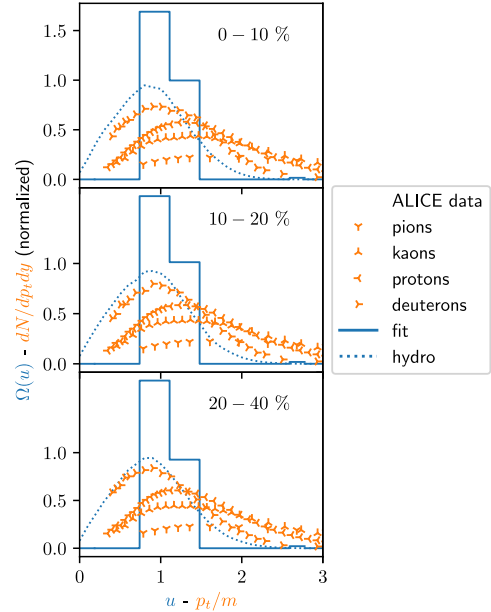


FIG. 5. (Color online) Symbols: Normalized distributions of p_t/m for pions, kaons, protons [42] and deuterons [66] in Pb+Pb collisions at $\sqrt{s_{\text{NN}}} = 2.76$ TeV in three centrality windows: 0-10%, 10-20%, 20-40%. Solid lines: normalized distribution of the fluid transverse velocity u resulting from a combined fit of these spectra using Eq. (10). Dotted lines: normalized distribution of u from our event-by-event hydrodynamic calculation. It is calculated in both cases using $p(u) \equiv \Omega(u) / \int_0^{\infty} \Omega(u') du'$.

the sum of identified particle spectra [42]. This is not completely trivial because the charged particle spectrum contains a significant contribution from Σ^{\pm} hyperons. Since Σ^{\pm} hyperons are not identified, their spectrum is not known. We estimate it using a procedure similar to that used by ALICE [67]. Specifically, we assume that the p_t spectrum of Σ^{\pm} hyperons is identical to that of Λ hyperons, which have the same strangeness content and a similar mass. The distribution dN/dp_t of Σ^{\pm} is then evaluated by multiplying dN/dp_t of Λ , which is measured [68], with the ratio Σ^{\pm}/Λ evaluated in the statistical model at this value of p_t . Fig. 6 shows the ratio of identified to unidentified particles in central Pb+Pb collisions, before and after including the contribution from Σ^{\pm} . One sees that this contribution significantly improves agreement at intermediate p_t . After it is included, agreement is at the level of a few percent, except at very low p_t . The apparent discrepancy at very low p_t is however likely to be explained by systematic errors, which are as large as 15% [42]. The conclusion is that the charged particle spectrum is well understood as the sum of identified-particle spectra.

We now extract the distribution of the transverse fluid velocity $\Omega(u)$ from the measured charged particle distri-

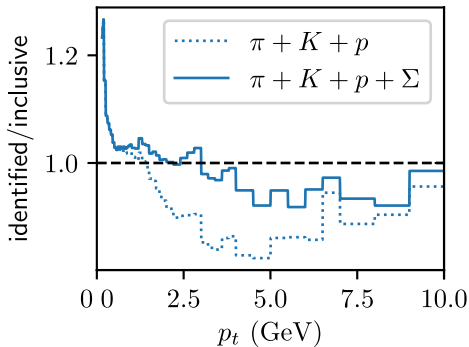


FIG. 6. (Color online) Ratio of the sum of identified particles to all charged particles [67] as a function of transverse momentum p_t , for Pb+Pb collisions at $\sqrt{s_{NN}} = 2.76$ TeV in the 0-5% centrality window. The dotted line includes pions, kaons and (anti)protons [42], while the full lines include the contribution of Σ^\pm hyperons, inferred from the measured Λ spectrum [68] (see text for details).

bution [67]. We again use Eq. (10), where we sum the contributions of pions, kaons, protons, and Σ baryons. The fit is excellent all the way up to $p_t = 6$ GeV/c, as shown in the right panels of Fig. 7.⁷ However, the corresponding values of $\Omega(u)$ differ significantly from those in Fig. 4 using data on identified particles. In addition to the peak around $u \sim 1$, already observed in Fig. 4, a second peak appears at $u \sim 0$, corresponding to a fluid at rest.

We now investigate the origin of the difference between Fig. 4 and Fig. 7. If Eq. (10) provided a perfect fit of identified spectra, then the value of $\Omega(u)$ would be identical in both cases (this is verified in Appendix A). But the combined fit to identified spectra is not perfect, and differences are to be expected. We have seen (Fig. 5) that the heaviest particles contain most of the information on $\Omega(u)$. Therefore, the combined fit to identified spectra is driven by the heaviest particles used in the fit (protons in the case of Fig. 3). On the contrary, the fit to the charged particle spectrum is driven by the lightest particles, namely, pions, which represent more than 80% of the yield (Fig. 2). To verify this, we carry out a fit of pion spectra using Eq. (10). The resulting $\Omega(u)$, shown as a dotted line in Fig. 7, also presents a peak around $u \sim 0$. This peak allows us to achieve good fits also at low p_t . It is interesting to note that the pion excess at low p_t can be interpreted as coming from a lump of fluid at rest, as if pions at low p_t did not experience the transverse boost imprinted by the pressure. This is qual-

⁷ The agreement at high p_t is again due to the small but nonvanishing $\Omega(u)$ in the highest bin $2.6 < u < 3$, as discussed above for identified particles.

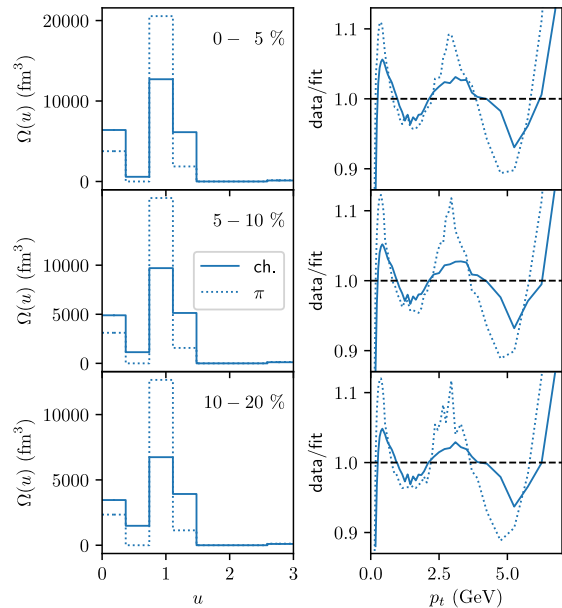


FIG. 7. (Color online) Left: Value of $\Omega(u)$ resulting from the fits to charged particle spectra [67] (solid lines) and pion spectra [42] (dotted lines) in Pb+Pb collisions at $\sqrt{s_{NN}} = 2.76$ TeV, using Eq. (10) summed over the relevant particle species (see text for details). Only three centrality windows are shown. Right: Ratio of the measured dN/dp_t divided by the best fit for charged particles (solid lines) and identified pions (dotted lines).

itatively similar to previous interpretations in terms of the formation of a Bose-Einstein condensate of pions [70] or a chiral condensate [59].

Note that a conventional hydrodynamic calculation will never produce a peak of $\Omega(u)$ at $u \sim 0$, because $\Omega(u) \propto u$ for small u , as seen in Fig. 4.⁸ A superfluid component would typically be needed [59].

IV. CENTRALITY DEPENDENCE OF FLUID VELOCITY FLUCTUATIONS

We finally study the centrality dependence of p_t spectra, and we discuss to what extent it is explained by hydrodynamics. Using our generalized blast-wave fit, we interpret the centrality dependence of p_t spectra as stemming from that of the fluid velocity distribution $\Omega(u)$. The information contained in $\Omega(u)$ can be expressed in

⁸ This behavior is easy to understand: The three dimensional distribution $\Omega(\mathbf{u})$ in Eq. (4) is typically continuous at finite $\mathbf{u} = 0$. Upon integration over the azimuthal angle ϕ_u , the integration measure $du_x du_y$ becomes $2\pi u du$, hence the distribution of the transverse fluid velocity is proportional to u .

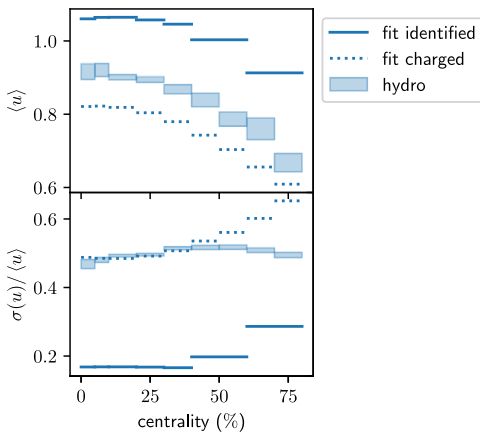


FIG. 8. (Color online) Centrality dependence of the mean value (top) and the relative standard deviation (bottom) of the fluid velocity distribution, as a function of centrality percentile, in Pb+Pb collisions at $\sqrt{s_{\text{NN}}} = 2.76$ TeV. They are evaluated using Eq. (13), where $\Omega(u)$ comes either from the fit to identified spectra (full lines in Fig. 4), from the fit to unidentified spectra (full lines in Fig. 7), or from the hydrodynamic calculation (dotted lines in Fig. 4). The width of the shaded band used to represent the result of the hydrodynamic calculation is the statistical error due to the finite number of hydrodynamic events, which is evaluated through jackknife resampling.

terms of its moments, defined by:

$$\langle u^n \rangle \equiv \frac{\int_0^\infty u^n \Omega(u) du}{\int_0^\infty \Omega(u) du}. \quad (13)$$

The mean fluid velocity $\langle u \rangle$ and the standard deviation $\sigma_u \equiv \sqrt{\langle u^2 \rangle - \langle u \rangle^2}$ encompass an information roughly equivalent to the mean value and the standard deviation of p_t . The advantage of choosing u as the variable, rather than p_t , is that comparison with hydrodynamic calculations is straightforward, and also more transparent.

Fig. 8 presents the centrality dependence of the mean fluid velocity, and of the relative standard deviation $\sigma_u/\langle u \rangle$. The mean value $\langle u \rangle$ extracted from data is smaller if one fits charged spectra than in one fits identified spectra. This is due to the value of $\Omega(u)$ at $u \sim 0$, which is large for charged particles (Fig. 7), and zero for identified particles (Fig. 4). The centrality dependence, however, is similar: the mean velocity mildly decreases as a function of centrality percentile. This decrease is quantitatively reproduced by our event-by-event hydrodynamic calculation, which lies between the results from fits to identified and charged spectra. This agreement is not surprising, since hydrodynamics is known to reproduce reasonably well the mild centrality dependence of the mean transverse momentum [2].

We finally discuss results for the relative standard deviation, shown in the bottom panel of Fig. 8. We have

already seen in Fig. 4 that fits to identified particle spectra return a distribution $\Omega(u)$ which is much narrower than an actual hydrodynamic calculation. Narrower implies a smaller $\sigma_u/\langle u \rangle$, which is seen in Fig. 8. The fits to charged particle spectra return values of $\sigma_u/\langle u \rangle$ in surprisingly good agreement with the hydrodynamic calculation up to 50% centrality, even though the distributions $\Omega(u)$ look different (compare the dotted lines in Fig. 4 and the solid lines in Fig. 7). The interesting, meaningful result is the mild centrality dependence of the relative standard deviation. Both fits (identified and charged) clearly show that it increases as a function of centrality percentile. A similar increase is seen in hydrodynamics, up to 50% centrality. The validity of hydrodynamics is expected to get worse as the centrality percentile increases, so that the discrepancies beyond 50% centrality are not significant. In hydrodynamics, the increase of $\sigma_u/\langle u \rangle$ can be ascribed to initial-state fluctuations, which are relatively larger in smaller systems, that is, in less central collisions. Our results show that these initial-state fluctuations, which were originally introduced in order to explain data on elliptic flow [71–74] and triangular flow [6], are also instrumental in explaining the centrality dependence of p_t spectra.

V. CONCLUSIONS

We have introduced an approximate treatment of freeze out in ideal hydrodynamics, which we have dubbed semi-Cooper–Frye freeze out, which gives transverse momentum distributions in reasonable agreement with a full hydrodynamic calculation. Within this approximation, dN/dp_t only involves the distribution of the fluid velocity at freeze out. Hence, this distribution of the fluid velocity can be directly obtained by fitting experimental data on dN/dp_t , in a way that generalizes usual blast-wave fits. Note that our procedure fully includes the feeddown from resonance decays. This generalized blast-wave approach allows us to fit p_t spectra all the way up to 6 GeV, while usual blast-wave fits or hydrodynamic calculations typically fail above 2 GeV.

We find that the most probable value of the transverse fluid velocity is 70% of the velocity of light in Pb+Pb collisions at $\sqrt{s_{\text{NN}}} = 2.76$ TeV. This value is comparable to that found in state-of-the-art hydrodynamic calculations. However, the shape of the fluid velocity distribution extracted from data differs qualitatively from that obtained in these calculations. In addition, it differs depending on whether one carries out a combined fit to identified spectra, or a fit to unidentified charged spectra. We have ascribed this difference to the fact that ideal hydrodynamics is unable to quantitatively explain all the data on p_t spectra. In particular, experimental data show a clear evidence of an excess of pions at low p_t , relative to ideal hydrodynamics. This excess suggests that the viscous correction to the momentum distribution is large at low momentum, unlike usually assumed in viscous hy-

hydrodynamic calculations.

We have studied the centrality dependence of p_t spectra in nucleus-nucleus collisions. Data on Pb+Pb collisions show that the distribution of the fluid velocity becomes broader as the centrality percentile increases. We have shown that this broadening is also present in hydrodynamic calculations, where it naturally arises as a

consequence of initial-state fluctuations.

ACKNOWLEDGEMENTS

We thank Giuliano Giacalone for discussions and for help with hydrodynamic calculations. We thank Aleksas Mazeliauskas for discussions and for help with the implementation of the FastReso code.

-
- [1] W. Busza, K. Rajagopal and W. van der Schee, *Ann. Rev. Nucl. Part. Sci.* **68**, 339-376 (2018) doi:10.1146/annurev-nucl-101917-020852 [arXiv:1802.04801 [hep-ph]].
- [2] F. G. Gardim, G. Giacalone, M. Luzum and J. Y. Ollitrault, *Nature Phys.* **16**, no.6, 615-619 (2020) doi:10.1038/s41567-020-0846-4 [arXiv:1908.09728 [nucl-th]].
- [3] E. Schnedermann, J. Sollfrank and U. W. Heinz, *Phys. Rev. C* **48**, 2462-2475 (1993) doi:10.1103/PhysRevC.48.2462 [arXiv:nucl-th/9307020 [nucl-th]].
- [4] J. Y. Ollitrault, *Phys. Rev. D* **46**, 229-245 (1992) doi:10.1103/PhysRevD.46.229
- [5] K. H. Ackermann *et al.* [STAR], *Phys. Rev. Lett.* **86**, 402-407 (2001) doi:10.1103/PhysRevLett.86.402 [arXiv:nucl-ex/0009011 [nucl-ex]].
- [6] B. Alver and G. Roland, *Phys. Rev. C* **81**, 054905 (2010) [erratum: *Phys. Rev. C* **82**, 039903 (2010)] doi:10.1103/PhysRevC.82.039903 [arXiv:1003.0194 [nucl-th]].
- [7] A. Kurkela, A. Mazeliauskas, J. F. Paquet, S. Schlichting and D. Teaney, *Phys. Rev. Lett.* **122**, no.12, 122302 (2019) doi:10.1103/PhysRevLett.122.122302 [arXiv:1805.01604 [hep-ph]].
- [8] F. Cooper and G. Frye, *Phys. Rev. D* **10**, 186 (1974) doi:10.1103/PhysRevD.10.186
- [9] J. Noronha-Hostler, G. S. Denicol, J. Noronha, R. P. G. Andrade and F. Grassi, *Phys. Rev. C* **88**, no.4, 044916 (2013) doi:10.1103/PhysRevC.88.044916 [arXiv:1305.1981 [nucl-th]].
- [10] H. Niemi, K. J. Eskola and R. Paatelainen, *Phys. Rev. C* **93**, no.2, 024907 (2016) doi:10.1103/PhysRevC.93.024907 [arXiv:1505.02677 [hep-ph]].
- [11] Y. Kanakubo, Y. Tachibana and T. Hirano, *Phys. Rev. C* **101**, no.2, 024912 (2020) doi:10.1103/PhysRevC.101.024912 [arXiv:1910.10556 [nucl-th]].
- [12] D. Teaney, J. Lauret and E. V. Shuryak, [arXiv:nucl-th/0110037 [nucl-th]].
- [13] H. Petersen, J. Steinheimer, G. Burau, M. Bleicher and H. Stöcker, *Phys. Rev. C* **78**, 044901 (2008) doi:10.1103/PhysRevC.78.044901 [arXiv:0806.1695 [nucl-th]].
- [14] J. E. Bernhard, J. S. Moreland, S. A. Bass, J. Liu and U. Heinz, *Phys. Rev. C* **94**, no.2, 024907 (2016) doi:10.1103/PhysRevC.94.024907 [arXiv:1605.03954 [nucl-th]].
- [15] B. Schenke, C. Shen and P. Tribedy, *Phys. Rev. C* **99**, no.4, 044908 (2019) doi:10.1103/PhysRevC.99.044908 [arXiv:1901.04378 [nucl-th]].
- [16] P. F. Kolb and U. W. Heinz, [arXiv:nucl-th/0305084 [nucl-th]].
- [17] J. Y. Ollitrault, *Eur. J. Phys.* **29**, 275-302 (2008) doi:10.1088/0143-0807/29/2/010 [arXiv:0708.2433 [nucl-th]].
- [18] R. Baier, P. Romatschke, D. T. Son, A. O. Starinets and M. A. Stephanov, *JHEP* **04**, 100 (2008) doi:10.1088/1126-6708/2008/04/100 [arXiv:0712.2451 [hep-th]].
- [19] P. Romatschke and U. Romatschke, doi:10.1017/9781108651998 [arXiv:1712.05815 [nucl-th]].
- [20] P. Romatschke and U. Romatschke, *Phys. Rev. Lett.* **99**, 172301 (2007) doi:10.1103/PhysRevLett.99.172301 [arXiv:0706.1522 [nucl-th]].
- [21] U. Heinz and R. Snellings, *Ann. Rev. Nucl. Part. Sci.* **63**, 123-151 (2013) doi:10.1146/annurev-nucl-102212-170540 [arXiv:1301.2826 [nucl-th]].
- [22] K. Dusling, G. D. Moore and D. Teaney, *Phys. Rev. C* **81**, 034907 (2010) doi:10.1103/PhysRevC.81.034907 [arXiv:0909.0754 [nucl-th]].
- [23] D. Molnar and Z. Wolff, *Phys. Rev. C* **95**, no.2, 024903 (2017) doi:10.1103/PhysRevC.95.024903 [arXiv:1404.7850 [nucl-th]].
- [24] N. Borghini and J. Y. Ollitrault, *Phys. Lett. B* **642**, 227-231 (2006) doi:10.1016/j.physletb.2006.09.062 [arXiv:nucl-th/0506045 [nucl-th]].
- [25] R. Hagedorn and J. Ranft, *Nuovo Cim. Suppl.* **6**, 169-354 (1968) CERN-TH-851.
- [26] K. A. Bugaev, *Phys. Rev. Lett.* **90**, 252301 (2003) doi:10.1103/PhysRevLett.90.252301 [arXiv:nucl-th/0210087 [nucl-th]].
- [27] D. Oliinychenko, P. Huovinen and H. Petersen, *Phys. Rev. C* **91**, no.2, 024906 (2015) doi:10.1103/PhysRevC.91.024906 [arXiv:1411.3912 [nucl-th]].
- [28] A. Mazeliauskas, S. Floerchinger, E. Grossi and D. Teaney, *Eur. Phys. J. C* **79**, no.3, 284 (2019) doi:10.1140/epjc/s10052-019-6791-7 [arXiv:1809.11049 [nucl-th]].
- [29] J. S. Moreland, J. E. Bernhard and S. A. Bass, *Phys. Rev. C* **92**, no.1, 011901 (2015) doi:10.1103/PhysRevC.92.011901 [arXiv:1412.4708 [nucl-th]].
- [30] P. F. Kolb, P. Huovinen, U. W. Heinz and H. Heiselberg, *Phys. Lett. B* **500**, 232-240 (2001) doi:10.1016/S0370-2693(01)00079-X [arXiv:hep-ph/0012137 [hep-ph]].
- [31] B. Schenke, S. Jeon and C. Gale, *Phys. Rev. C* **82**, 014903 (2010) doi:10.1103/PhysRevC.82.014903

- [71] M. Miller and R. Snellings, [arXiv:nucl-ex/0312008 [nucl-ex]].
- [72] R. Andrade, F. Grassi, Y. Hama, T. Kodama and O. Socolowski, Jr., Phys. Rev. Lett. **97**, 202302 (2006) doi:10.1103/PhysRevLett.97.202302 [arXiv:nucl-th/0608067 [nucl-th]].
- [73] B. Alver *et al.* [PHOBOS], Phys. Rev. Lett. **98**, 242302 (2007) doi:10.1103/PhysRevLett.98.242302 [arXiv:nucl-ex/0610037 [nucl-ex]].
- [74] H. Holopainen, H. Niemi and K. J. Eskola, Phys. Rev. C **83**, 034901 (2011) doi:10.1103/PhysRevC.83.034901 [arXiv:1007.0368 [hep-ph]].

Appendix A: Test of the fitting algorithm

We test the validity of our fitting algorithm in the following way. We choose a distribution $\Omega(u)$ as input. We then compute a fake dN/dp_t containing either pions + kaons + protons, pions alone or all charged particles with this $\Omega(u)$. We then check that the fit to this dN/dp_t using Eq. (10) recovers the correct value of the input distribution $\Omega(u)$. This is shown in Fig. 9 for two different values of the input distribution. The reconstructed $\Omega(u)$ agrees perfectly with the input, irrespective of whether whether the fake dN/dp_t contained pions+kaons+protons, pions alone or all charged particles.

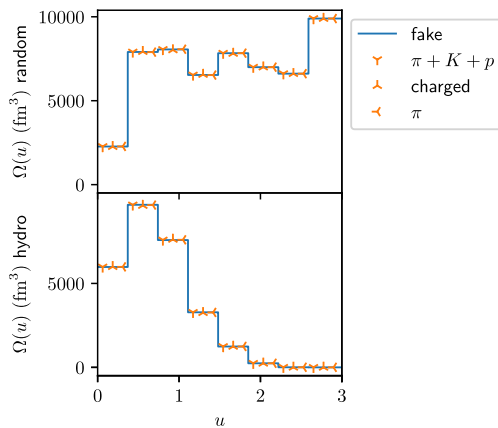


FIG. 9. (Color online) Comparison between the input value of $\Omega(u)$ (full lines) and the result returned by the fit to the fake dN/dp_t containing either pions, kaons and protons (down pointing star), pions alone (left pointing star) or all charged particles (pions, kaons, protons and Σ^\pm) (up pointing star) to the spectrum dN/dp_t using Eq. (10). The input value is a discrete distribution, for the sake of consistency with the results shown in this paper. The top panel corresponds to an irregular $\Omega(u)$ chosen randomly, and the bottom panel to a regular $\Omega(u)$ similar to that obtained in an actual hydrodynamic simulation.